Towards a General Understanding of Hydrothermal Polymerization of Polyimides

Journal:	*Polymer Chemistry*
Manuscript ID:	PY-ART-02-2015-000231.R1
Article Type:	Paper
Date Submitted by the Author:	09-May-2015
Complete List of Authors:	Baumgartner, Bettina; Technische Universität Wien, Institute of Materials Chemistry Puchberger, Michael; Technische Universität Wien, Institute of Materials Chemistry Unterlass, Miriam; Vienna University of Technology, Institute of Materials Chemistry

Towards a General Understanding of Hydrothermal Polymerization of Polyimides†

Bettina Baumgartner[a], Michael Puchberger[a], and Miriam M. Unterlass*[a]

Received Xth XXXXXXXXXX 20XX, Accepted Xth XXXXXXXXX 20XX
First published on the web Xth XXXXXXXXXX 200X
DOI: 10.1039/b000000x

Hydrothermal polymerization (HTP) has been recently established as a novel route to synthesize polyimides of outstanding crystallinity. In this contribution, we lay out the basic theoretical and experimental framework for understanding the mechanistic underpinnings of this process. For this purpose, we hydrothermally synthesize two representative polyimides that are known to form amorphous polymers when synthesized classically. Hydrothermal polymerization, in contrast, yields unprecedented crystallinity after only two hours. The co-monomers diamine and dianhydride form monomer salts *via* acid-base reaction when brought in contact in water. We show that the physicochemical properties of the crystalline monomer salts (*i.e.* solubility, solid-state polymerization temperature) are important factors for the crystallinity and the morphology of the corresponding hydrothermally synthesized polyimide. We develop a mechanistic model of hydrothermal polymerization processes allowing us to relate the polymerization parameters (concentration, reaction temperature, reaction time) to the obtained polyimide crystallinity and morphology. By adjusting the parameters, the achieved crystallinity can be further increased and high morphological homogeneity can be obtained. We believe that the developed mechanistic picture is applicable for the hydrothermal polymerization of any polyimide.

1 Introduction

Aromatic polyimides (PIs), or Arimids, are among the most important high-performance polymers. They are characterized by outstanding thermal and mechanical performance, and chemical resistance. Their technological relevance ranges from microelectronics, where they are used *e.g.* as dielectrics in printed circuit boards,[1] components in scientific instrumentation, *e.g.* as window material in X-Ray diffractometers,[2] to applications in aerospace: the solar sail of the Japanese spacecraft IKAROS, for instance, is a polyimide sheet of 20 m in diameter and only 7.5 μm in thickckness.[3] The classical syntheses of PIs are employing high-boiling and often toxic solvents (*e.g.* cresols, dimethylformamide, dimethylacetamide), toxic catalysts (*e.g.* isoquinoline) and high process temperatures of up to several hundred °C.[4,5] Classical PI syntheses involve poly(amic acid) (PAA) intermediates, which can be isolated (Scheme 1A). For technological applications, PIs are often additionally cured in the solid-state at up to 500 °C to further increase their average molecular weights and crystallinity.[6] Despite their technological relevance and the fact

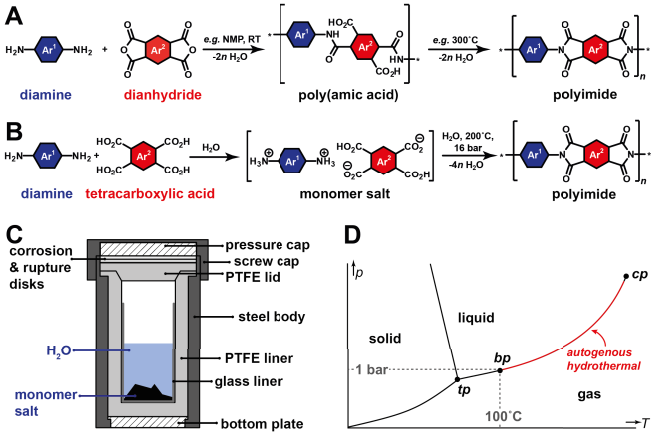

Scheme 1 This scheme has been revised. Classical and hydrothermal syntheses of aromatic polyimides. **A:** Classical pathway: diamine and dianhydride first form a poly(amic acid) intermediate, which further condenses to the PI. **B:** Hydrothermal polymerization (HTP): diamine and teracarboxylic acid react to a monomer salt (*via* acid-base reaction), which is polymerized to the PI under HT conditions. **C:** Schematic of a non-stirred autoclave used to generate HT conditions. **D:** Phase diagram of H_2O showing the HT region situated at $T > 100$ °C and $p > 1$ bar, but below the supercritical region (critical point *cp* (374 °C, 220 bar). If the pressure in an autoclave arises autogenously, one works exactly at the liquid vapor line (red).

† Electronic Supplementary Information (ESI) available: experimental details, TGA, FT-IR-ATR, NMR, solubility tests, SEM, PXRD. See DOI: 10.1039/b000000x/

[a] *Technische Universität Wien, Institute of Materials Chemistry, Department of Applied Inorganic Synthesis, Getreidemarkt 9/BC/2, A-1060 Vienna, Austria. E-mail: miriam.unterlass@tuwien.ac.at*

that many PIs are commercially available, little progress has been made in the last decades towards alternative polymerization techniques. The few reported non-classical approaches are: (*i*) phase-separation of PAA oligomers in apolar solvents such as liquid paraffins at around 300 °C,[7] (*ii*) the polymerization of dianhydrides and diisocyanates *via* decarboxylation,[8] (*iii*) heterophase polymerization of dianhydride and diamine in ionic liquids,[9] and (*iv*) the rearrangement of polyisoimides.[10] We have recently broadened the range of non-classical syntheses of PIs by two techniques: solvent-free, solid-state polycondensation (SSP), and hydrothermal polymerization (HTP).[11–13] HTP is a geomimetic approach, inspired by the condensation of silicic acids to silicates in hydrothermal veins in the earth's crust.[14] In contrast to classical procedures that rely on high-boiling, toxic solvents and catalysts, HTP uses nothing but the monomers and water and is thus inherently environmentally friendly.

In HTP, the comonomers dianhydride (or tetracarboxylic acid) and diamine inevitably form a monomer salt intermediate, which is a diamminium dicarboxylate dicarboxylic acid. This monomer salt then undergoes polycondensation in water at increased temperatures and pressures (typical HTP conditions are 200 °C and 16.7 bar, see Scheme 1B). As the monomer salt formation is unavoidable,[13] we typically prepare the monomer salt as starting compound. This is not crucial but advisable: The preparation of a monomer salt (including its purification by washing and filtration, which removes excess monomers) generates a precursor of ideal stoichiometry that is needed for obtaining high conversion and degrees of polymerization according to *Carothers'* Law.[15]

The elevated T- and p- conditions in HTP are generated using closed steel tank reactors, so-called autoclaves (Scheme 1C). Typically, a dispersion of the monomer salt in H_2O is enclosed in an autoclave at room temperature (RT) and placed in an oven at the reaction temperature T_R, which must be above 100 °C to be in the HT regime. Since the autoclave is a closed system, autogenous pressure builds up, thus, the system operates at the liquid-vapor line of water (Scheme 1D). Similar to the hydrothermal synthesis of highly crystalline silicates, we have recently shown that the fully aromatic polyimide poly(*p*-phenylene pyromellitimide) (PPPI) can be obtained with impressive crystallinity by HTP.[11]

In this contribution, we present the hydrothermal synthesis of two PIs based on the monomer benzophenone-3,3',4,4'-tetracarboxylic acid (BTA) in combination with two different diamine co-monomers. BTA-based PIs have been reported to show promising properties for a wide-range of applications including good permselectivity,[16,17] and a high amount of H-bonding acceptor functions (imide and benzophenone carbonyl moieties).[18] We chose these BTA-based systems as (*i*) they are reported to be amorphous polymers when classically synthesized,[19,20] and (*ii*) their monomer salts are soluble – to a small extent – below 100 °C in water. The fact that they are soluble in the subhydrothermal regime influences both the crystallinity and the morphology of the final PIs. Using micromorphological analysis and X-Ray diffraction, we are able to develop a mechanistic, and as we believe generally applicable picture of HTP.

2 Results and Discussion

We investigated the synthesis of two PIs based on benzophenone-3,3',4,4'-tetracarboxylic acid (BTA) in combination with the amines *p*-phenylene diamine (PDA) and benzidine (Bz) (Scheme 2). The monomer salts were first synthesized by vigorous stirring of the respective diamine with an equimolar amount of BTA in water for 2 h at 80 °C, as previously reported.[11] FT-IR-ATR analysis (ESI†) of both products revealed the coexistence of the typical monomer salt modes ($\tilde{\nu}_{as}$(Ar-NH_3^+) ≈ 2830 cm^{-1}, $\tilde{\nu}_s$(Ar-NH_3^+) ≈ 2580 cm^{-1}, $\tilde{\nu}$(C=O, Ar-CO_2H) ≈ 1680 cm^{-1}, $\tilde{\nu}_{as}$(C=O, Ar-CO_2^-) ≈ 1605 cm^{-1}, and $\tilde{\nu}_s$(C=O, Ar-CO_2^-) ≈ 1570 cm^{-1}) with the characteristic imide modes ($\tilde{\nu}_{as}$(C=O) ≈ 1775 cm^{-1}, $\tilde{\nu}_s$(C=O) ≈ 1720 cm^{-1}, and $\tilde{\nu}_s$(C−N) ≈ 1365 cm^{-1}). In addition, we did not find any amide modes, underlining that there are no isolable PAA intermediates occurring in HTP. The presence of imide modes clearly indicates that both monomer salts synthesized at 80 °C had already started to dissolve and polymerize. In order to avoid prepolymerization at the precursor level, we modified the monomer salt synthesis to stirring the co-monomers for 1 day at RT. The monomer salts were isolated as pale powders and purified by filtration and thorough washing with cold deionized water. From FT-IR-ATR analysis of the dried powders, we find perfectly clean monomer salts showing neither modes related to the cyclic imide nor to the non-ionized monomers (ESI†). The monomer salts were soluble in several protic and aprotic polar solvents (ESI†), thereby allowing for solution NMR analysis (ESI†). From

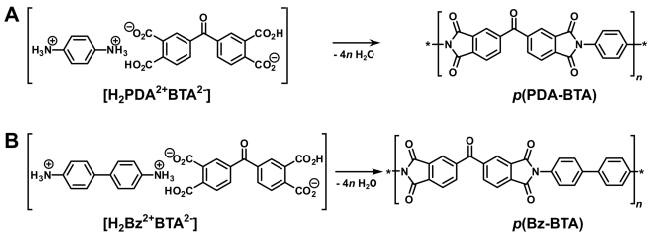

Scheme 2 Monomer salts and polyimides used in this study. **A:** The monomer salt of benzophenone-3,3',4,4'-tetracarboxylic acid (BTA) and the diamine *p*-phenylene diamine (PDA), thus [$H_2PDA^{2+}BTA^{2-}$], and the resulting polyimide *p*(PDA-BTA). **B:** The monomer salt of BTA and the diamine benzidine (Bz), thus [$H_2Bz^{2+}BTA^{2-}$], and the resulting polyimide *p*(Bz-BTA).

^{1}H-NMR, we find good agreement with a equimolar ratio of BTA to each diamine, respectively, and exclusively peaks related to amminium protons, but no remaining amine peaks. Both monomer salts are thus diamminium-dicarboxylate-dicarboxylic acid salts. Consequently, the formulae of the studied salts are: [$H_2PDA^{2+}BTA^{2-}$] and [$H_2Bz^{2+}BTA^{2-}$].

For HTP, the dried monomer salts were redispersed in deionized water inside glass liners and transferred to PTFE-lined steel autoclaves (*cf.* Scheme 1). The autoclaves were placed in an oven that was preheated to 200 °C, and kept there for different reaction times (t_R = 1 h, 2 h, 4 h and 12 h). After t_R, the autoclaves were quenched in cold tap water to quickly cool them back to RT, washed with cold deionized H_2O and dried over P_2O_5 in a desiccator. After HTP, we typically find two product phases in the glass liner: a yellowish bottom phase (the *a*-phase), and a less dense, dark brown *b*-phase.[11] The *a*-phase accounts for the majority of the product's mass and is of yellow-brownish color for *p*(PDA-BTA) and yellow-greenish color for *p*(Bz-BTA) (see ESI† for photographs). As previously reported for PPPI, the *b*-phase originates from polymerization and crystallization in solution in the HT regime, whereas the *a*-phase is composed of PI that also polymerizes in solution, but crystallizes on earlier formed PI crystallites that act as seed particles.[11]

For all characterizations we analyze both the *a*- and the *b*-phases to account for eventual differences. We used only cold deionized water for washing the products prior to all analyses in order to be able to properly evaluate *e.g.* remaining monomer salt (which would be removed by washing with other solvents, see ESI†). After the characterizations, the products' solubilities in various solvents were tested (ESI†). All polyimide *a*- and *b*- phases were insoluble in any solvent other than concentrated sulfuric acid. From FT-IR-ATR analysis of the products synthesized at different reaction times (ESI†), it becomes clear that HTP of both [$H_2PDA^{2+}BTA^{2-}$] and [$H_2Bz^{2+}BTA^{2-}$] yields fully imidized PIs (absence of monomer salt modes and potential end-groups, presence of imide modes) after only 1 h at 200 °C and 16.7 bar (ESI†).

Scanning electron microscopy (SEM) revealed a striking morphological difference between the monomer salts (Fig. 1A,F) and the polyimide *a*- and *b*-phases (Fig. 1B-E, G-J). Fig. 1 shows the PI products for t_R = 2 h and 12 h (for SEM of t_R = 1 h, 4 h and overview images see ESI†). Where [$H_2PDA^{2+}BTA^{2-}$] appears as polycrystalline powder (Fig. 1A), *p*(PDA-BTA) shows dense roundish cauliflower-like morphologies coexisting with spherical particles covered with naonocrystallites in the *a*-phase (Fig. 1B,D), and microflower morphologies in the *b*-phase, for all tested t_R (Fig. 1C,E). While the morphologies of the *b*-phase seem not to vary with time, the morphological homogeneity of the *a*-phases increases with t_R (ESI†). [$H_2Bz^{2+}BTA^{2-}$] has the appearance of polycrystalline crystallites in SEM (Fig. 1F). The morphology of *p*(Bz-BTA) is strikingly different from the monomer salt and also evolves with t_R: the *a*-phase shows highly size-monodisperse aggregates of platy crystallites of *ca.* 1 μm at t_R = 1 h (ESI†). With increasing t_R, these grow into a fascinating morphology: we consistently find flat flower-shape crystallites with rounded petals, which are decorated with smaller crystallites exclusively on the petals' rims (Fig. 1G). At the highest t_R (12 h), these rounded flowers develop into denser roundish aggregates (Fig. 1I). The *p*(Bz-BTA) *b*-phases are composed of cauliflower-like aggregates and microflowers (Fig. 1H,J), which – like the *p*(PDA-BTA) *b*-phases – don't seem to morphologically evolve with t_R.

All these well-ordered morphologies are already indicative of high crystallinity. The flower-shaped PI morphologies are, as we have shown previously, the result of a geometrical selection process during crystal growth.[11] But where do the cauliflower-like morphologies (*cf.* Fig. 1B,D,H,J) originate from? Their form suggests the growth of PI crystallites on spherical objects. These spherical macroscopic nuclei are in fact PI particles that form by polymerization below 100 °C, *i.e.* in the subhydrothermal regime, as we will discuss in detail in section **2.1**.

To further substantiate the high crystallinity indicated by SEM, we performed powder X-ray diffraction (XRD) for both monomer salts and all polyimides. XRD reveals outstanding crystallinity for both *a*- and *b*-phases of both polyimides (Fig. 2A,B for t_R = 12 h; for other t_R see ESI†). This is especially noteworthy as both PIs are known as amorphous and non-crystallizing polymers.[7,20] Kimura and co-workers synthesized highly crystalline *p*(PDA-BTA) using phase separation techniques. Surprisingly, *p*(PDA-BTA) synthesized via HTP does exceed their reported crystallinity: we find several additional reflexes (Fig. 2A, emphasized by blue arrows).

Comparison of the diffractograms for different reaction times of the two polyimides, respectively, reveals that the crystallinity of *b*-phases does not change significantly with t_R, for T_R = 200 °C. This is in agreement with SEM, where no morphological changes of the *b*-phases were observed with t_R. For the *a*-phases of both polymers, however, we do observe that the crystallinity increases with increasing t_R (ESI†). From XRD, *a*- and *b*-phases are different from each other in three points: (*i*) the *b*-phases show sharper reflexes than the *a*-phases synthesized at the same t_R. (*ii*) The *b*-phases show additional reflexes. There is one additional reflex at 24° (2θ) for *p*(PDA-BTA) (Fig. 2A, light blue arrow; and ESI†), and for *p*(Bz-BTA) the reflex at 22° (2θ) of the *a*-phases is not present in the *b*-phases, which instead show two reflexes at 22.5° and 23° (2θ) (Fig. 2B, light blue arrows; and ESI†). (*iii*) The *b*-phases show reflexes of each respective monomer salt for t_R = 1 h (ESI†).

All three points indicate that the *b*-phase is formed by HTP in solution as only polymerization mechanism: The *b*-phases

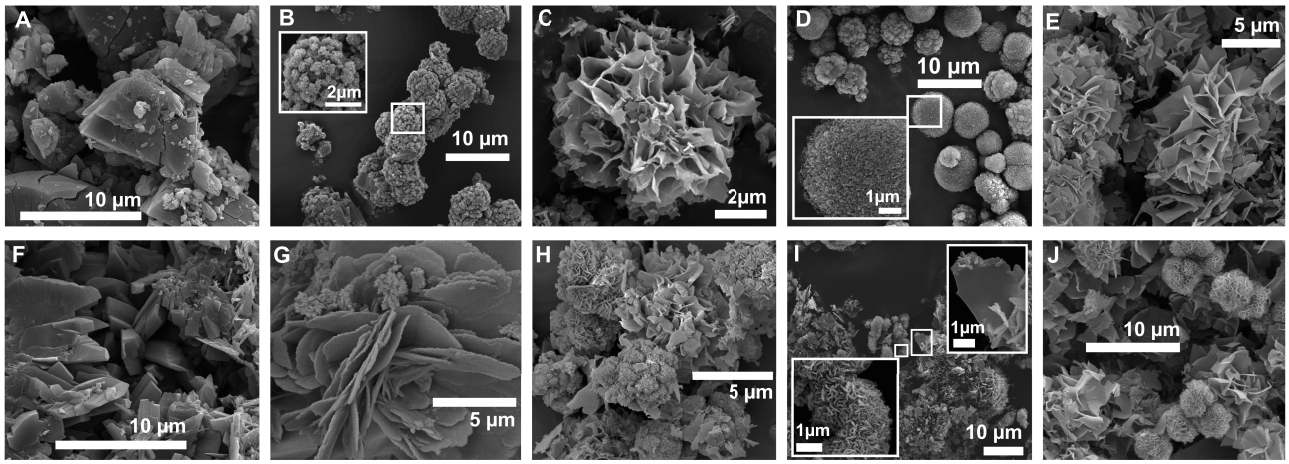

Fig. 1 This figure caption has been changed SEM images of monomer salts synthesized at RT and polyimides synthesized at 200 °C. **A:** $[H_2PDA^{2+}BTA^{2-}]$; **B-C:** *p*(PDA-BTA), t_R = 2 h, *a*-phase (**B**), *b*-phase (**C**); **D-E:** *p*(PDA-BTA), t_R = 12 h, *a*-phase (**D**), *b*-phase (**E**); **F:** $[H_2Bz^{2+}BTA^{2-}]$; **G-H:** *p*(Bz-BTA), t_R = 2 h, *a*-phase (**G**), *b*-phase (**H**); **I-J:** *p*(Bz-BTA), t_R = 12 h, *a*-phase (**I**), *b*-phase (**J**).

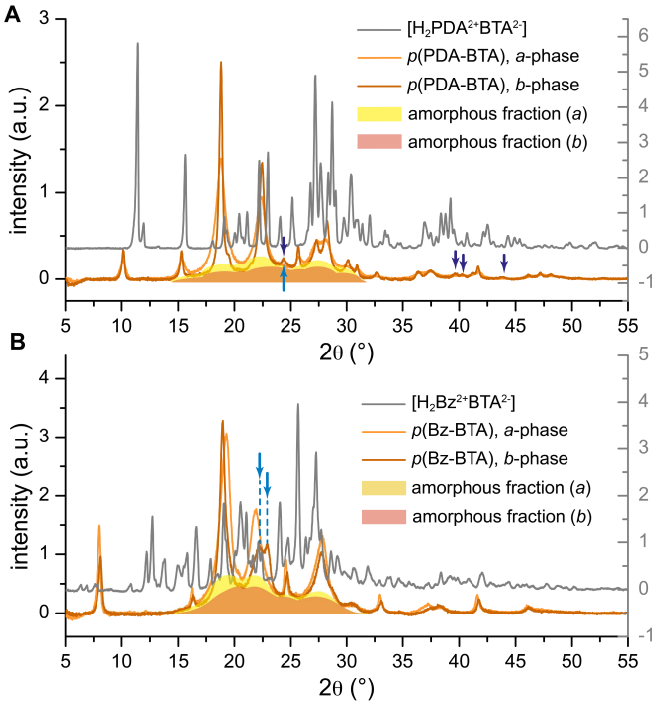

Fig. 2 This figure caption has been changed Powder-diffractograms of the dried *a*- and *b*-phases after HTP ($T_R = 200$ °C, $t_R = 12$ h); The amorphous fractions are illustrated by yellow areas **A:** *p*(PDA-BTA); **B:** *p*(Bz-BTA).

form by simultaneous polymerization and crystallization,[11] from dissolved BTA^{2-} and H_2PDA^{2+} and H_2Bz^{2+} ions, respectively. After 1 h, the polymerization is not complete. Thus when the autoclave is cooled back to RT, the respective monomer salt crystallizes again and since the amount is relatively small, it is only visible *via* XRD but not *via* FT-IR-ATR (higher sensitivity of XRD). As the *b*-phases are basically exclusively formed by HTP, which is complete at 1 h $\leq t_R \leq$ 2 h, neither their crystallinity nor their morphology is affected by t_R.

Both PIs show impressive crystallinity from XRD. However, there is a small amorphous background for *p*(PDA-BTA) and *p*(Bz-BTA) (illustrated by colored areas in Fig. 2). We find that the amorphous background of the *b*-phases is always smaller than the one of the *a*-phases, again underlining the higher crystallinity of the *b*-phases. In the previously reported case of PPPI, we did not observe any amorphous background.[11] As detailed in the following, we argue that the emergence of the amorphous background observed in this study is a consequence of (*i*) solubility and polymerization of the monomer salts in the subhydrothermal regime (section **2.1**), and (*ii*) of solid-state polymerization taking place in dispersion in the HT regime (section **2.2**).

2.1 Origin and consequences for PI crystallinity of monomer salt solubility in the subhydrothermal regime

Preparation of the monomer salts at 80 °C had lead to prepolymerization. More generally speaking, the monomer salts start to dissolve and polymerize at a reaction temperature with RT $\leq T_R \leq$ 100 °C, *i.e.* in the sub-hydrothermal (sHT) regime.

Where polymerzation in the HT regime leads to crystalline PIs,[11] polymerization in the sHT regime yields amorphous PIs. To verify this, we refluxed the two monomer salts for 1 h and 12 h, respectively, in water, and analyzed the crude products by FT-IR-ATR and XRD. FT-IR-ATR analysis shows both monomer salt and imide modes for both systems (ESI†), and XRD reveals strong monomer salt reflexes on top of indeed broad amorphous halos (ESI†). SEM analysis of the crude products after refluxing for 12 h shows big pieces that seem to be built up of small roundish particles (ESI†). Thus, the subhydrothermal polymerization (sHTP) of monomer salts is best described as typical solution polycondensation leading to spherical PI particles: The freshly formed PI is physicochemically very different from the continuous phase and thus tries to minimize its surface free energy, resulting in a spherical shape (*cf.* section **2.3**). The observation that polymerization in the subhydrothermal regime (sHTP) yields an amorphous PI product, while HTP yields a crystalline product is indeed curious. In order to tackle this question, one needs to first compare the crystalline to the amorphous product. A crystalline linear PI can be best understood as chains of a homogeneous conformation that are arranged over a long-range. An amorphous PI is best described as an array of chains of inhomogeneous conformation (*e.g.* irregularly kinked chains). Due to the inhomogeneity of the chain conformations, the PI chains cannot pack in a lon-range ordered array, but are rather randomly packed (Scheme 3). The crystalline product of a certain PI represents the thermodynamic reaction product, while the amorphous counterpart is the kinetic product (Scheme 3). Thus, the fact that sHTP leads to amorphous PI, while HTP yields crystalline PI allows for the conclusion that HTP conditions favor the thermodynamic product, and the crystalline PI is formed under thermodynamic reaction control. The concept of thermodynamic *vs.* kinetic reaction control for crystalline *vs.* amorphous product has been established by *Yaghi* and coworkers for covalent organic and metal organic frameworks (COFs and MOFs).[21–23] In the synthesis of both COFs and MOFs, the obtainment of the crystalline, thermodynamic product is however coupled to the use of dynamic covalent bonds between monomeric units. Specifically, the amorphous product forms first in COF and MOF syntheses, and the possibility of a reversible linking chemistry does then allow for the monomeric units to detach from and reattach to each other until the thermodynamic product is formed. The cylclic imide linkage in PIs is however essentially irreversible[11], and the concept of linker reversibility does thus not apply here. We previously attempted to recrystallize preformed PIs hydrothermally, which was not successful,[11] which shows that the cyclic imide moiety is irreversible even under HT conditions. HTP of polyimides is closely related to the natural formation of silicates by polycondensation of silicic acid species (*cf.* section **1**). Hydrothermal synthesis of silicates also yields crystalline products, and most interestingly, the Si-O bond is also essentially irreversible. We thus conclude that HT conditions might directly favor the thermodynamic product in polycondensation with water as byproduct. Little is understood about the underpinings, but we believe that the increased temperatures and pressures (and consequently increased number of molecular collisions), in combination with the fact that the monomers are dissolved in HTP, might allow for overcoming the activation energy towards the thermodynamic product directly. The activation energy towards the kinetic product is smaller, and the moderate temperature and pressure in the sHT regime might only allow for yielding the kinetic, amorphous PI product.

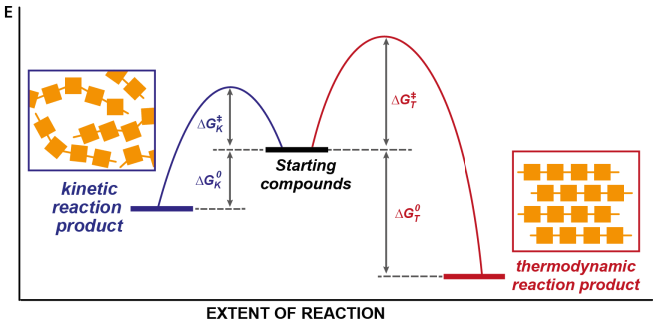

Scheme 3 Thermodynamic *vs.* kinetic reaction control for crystalline *vs.* amorphous PIs. **Left**: The amorphous PI represents the kinetic product. Reaching the kinetic product requires an activation energy $\Delta G_K^{\ddagger}$, and the overall free energy difference between the starting compounds and the kinetic product is ΔG_K^0. **Right**: The crystalline PI represents the thermodynamic product. The activation energy towards the thermodynamic product, $\Delta G_T^{\ddagger}$ is higher than $\Delta G_K^{\ddagger}$, and the overall free energy gain when reaching the thermodynamic product, ΔG_T^0 also exceeds ΔG_K^0.

Due to our experimental procedure, where we load an autoclave with a monomer salt dispersion at RT and then place it in an oven preheated to T_R, the monomer salt dispersion inevitably passes the sHT regime while heating up. The medium H_2O itself should heat up very quickly. However, the interfaces between the dissimilar materials in our experimental set-up slow down the heat conduction.[24] When heating up the autoclave, thermal conduction has to occur between (from outside to inside) air to steel to PTFE to glass to water (*cf.* Scheme 1C). Given the temperature difference of ca. 175 °C (for T_R = 200 °C) and the different materials present, we estimate the heating time t_h until the reaction mixture reaches T_R to be 30–40 min.

We conclude that (*i*) dissolution of the monomer salt and polymerization in the sHT regime takes place; (*ii*) sHTP indeed yields amorphous products; and (*iii*) the salts cannot fully dissolve and polymerize during 1 h at 100 °C. It is inevitable that the reaction mixture passes the sHT regime during heating, which accounts for a small amorphous fraction

in the final product after HTP (Scheme 4A,B). For the case of the previously reported HTP of PPPI, where we did not observe any amorphous fraction, we conclude that the corresponding monomer salt was virtually insoluble in H_2O in the sHT regime.

If a monomer salt already starts to dissolve and polymerize at relatively low temperatures, the sHTP pathway will occur during heating of the autoclave, which cannot be avoided. Thus, such a monomer salt will lead to an amorphous fraction in classical HTP whose size scales with the extent to which it *dissolves and polymerizes* during heating of the autoclave. Here, it is important to differentiate between mere dissolution and dissolution *and* subsequent polymerization: if n mol of a monomer salt dissolve during heating, but only x mol (with $x < n$) can polymerize in the sHT regime, $(n - x)$ mol of monomer salt are already dissolved in the sHT regime, but pass to the HT regime without polymerization. They then polymerize in the HT regime where they yield crystalline PIs. Thus, the solubility of the monomer salt in the sHT area cannot be considered alone for the amorphous fraction.

Let us now briefly discuss why [$H_2PDA^{2+}BTA^{2-}$] and [$H_2Bz^{2+}BTA^{2-}$] are soluble in the sHT regime, while the monomer salt of PPPI ([$H_2PDA^{2+}PMA^{2-}$])[11] was not. We therefore need to consider solubility at a very fundamental level. For the dissolution of an organic salt, one has to consider two energetic contributions: (*i*) the energy required to break up the salt crystal, which has to be expended; and (*ii*) the solvation energy of the organic ions when dissolved, which is released. The solvation energy is basically determined by the number and strength of bonds (here: H-bonds) that are formed between the solute (the organic ions) and the solvent molecules (here: H_2O). The energy required to break the monomer salt's crystal lattice depends on how strongly the organic ions in the lattice are bound to each other, *i.e.* the number of interactions (H-bonds, Van der Waals interactions, pi-pi interactions) per organic ion and thus the distances between organic ions. Comparing the monomer salt of PPPI ([$H_2PDA^{2+}PMA^{2-}$]) to the BTA^{2-} containing salts in this study, one would expect the smaller ions in [$H_2PDA^{2+}PMA^{2-}$] to be solvated more effectively. Thus, we expect [$H_2PDA^{2+}PMA^{2-}$] to form a crystal of relatively high lattice energy, compared to the lattice energies of BTA^{2-}-containing monomer salts. In conclusion, the question whether and to what extent a monomer salt is soluble in the sHT regime depends on the energetic contributions (lattice energy and energy of solvation) of each precise monomer salt. Thus, there is currently no simple rule of thumb to predict if a monomer salt will be soluble in the sHT regime or not.

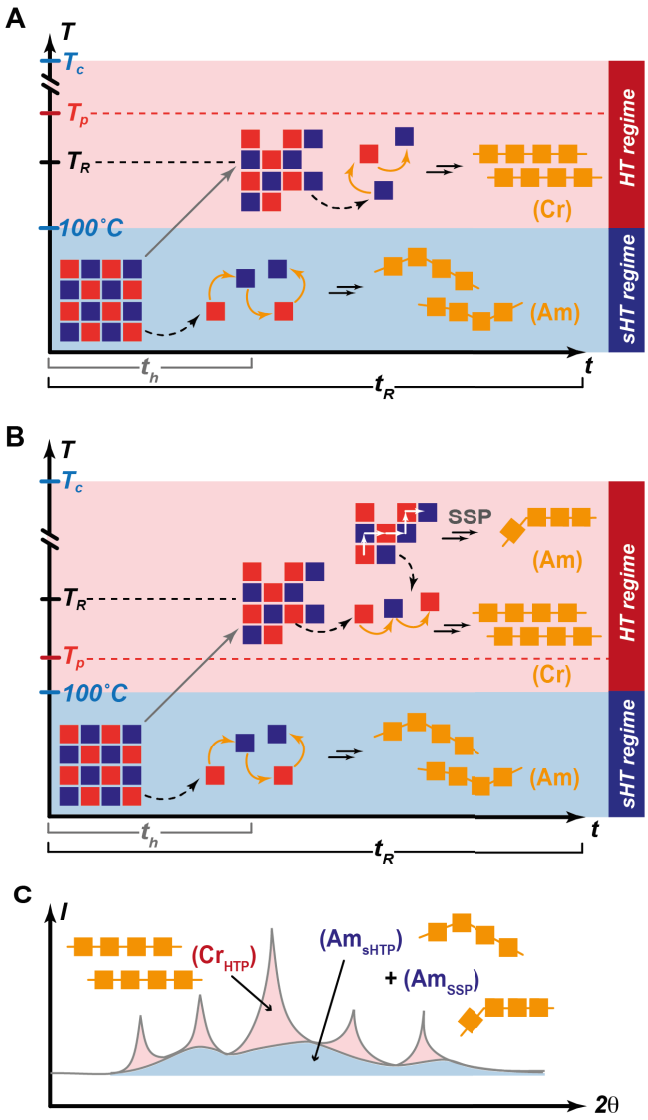

Scheme 4 Origin of amorphous and crystalline fractions in HTP of BTA-based polyimides. **A:** In HTP carried out below the solid-state polymerization temperature of the monomer salt (T_p), a part of the monomer salt can dissolve in the sub-hydrothermal (sHT) regime during the time of heating (t_h) of the autoclave. Polymerization in the sHT area yields amorphous products. The majority of the monomer salt is dissolved and polymerized in the HT regime and thus leads to highly crystalline PIs. **B:** HTP at $T_R > T_p$ also yields amorphous PI from sHTP and crystalline PI from HTP. If there is still non-dissolved monomer salt left, it can undergo solid-state polymerization (SSP), which leads to amorphous products. **C:** Schematic of a diffractogram containing both a crystalline fraction (from PI formed by HTP) and amorphous halos (from PI formed by sHTP and SSP).

2.2 Solid-state polymerizations in the HT regime and their effect on crystallinity

In addition to sHTP, there is a second polymerization mechanism that has to be considered: solid-state polymerization (SSP). Monomer salts of the diamminium-dicarboxylates-dicarboxylic acid type can undergo SSP when they are heated to their specific polymerization temperature T_p.[12] The T_p can be easily identified *via* thermogravimetric analysis (TGA), where one observes a mass loss that corresponds to the liberation of two equivalents of H_2O per imide ring (thus four equivalents per repeating unit). In combination with a differential scanning calorimetry (DSC) measurement with several heating and cooling cycles, one can identify this mass loss at T_p as a reaction peak only present in the first heating ramp. After the first heating ramp, the monomer salt has completely transformed to PI and all subsequent heating-cooling cycles show a flat curve, clearly underlining that the mass loss at T_p is associated with an irreversible reaction.[12] Therefore, if one performs HTP at $T_R \geq T_p$, non-dissolved monomer salt can undergo SSP (in dispersion in the medium H_2O). For PPPI, $T_p \approx 205 - 210$ °C, and with $T_R = 150$, 180 and 200 °C, we were previously operating below T_p of the corresponding monomer salt.[11] In order to clarify if SSP might be a possible polymerization pathway here, we performed TGA of both monomer salts used in this study (ESI†). The temperatures of polymerization were identified as $T_p([H_2PDA^{2+}BTA^{2-}])$ = 149 °C and $T_p([H_2Bz^{2+}BTA^{2-}])$ = 172 °C. Therefore, with T_R = 200 °C, one operates above T_p of both systems. PIs obtained *via* SSP are typically much less crystalline than from HTP.[12] In order to verify if this is also the case for the BTA-based systems, we carried out SSP for 12 h at 200 °C of the dried monomer salts (for experimental procedure see ESI†). XRD (ESI†) reveals that SSP yields fully amorphous *p*(PDA-BTA) and semicrystalline *p*(Bz-BTA) with a major amorphous background. Overall, we conclude that (*i*) pure SSP yields fully (*p*(PDA-BTA)) and mainly amorphous (*p*(Bz-BTA)) products. (*ii*) At the chosen T_R = 200 °C, we operate above solid-state T_p of both systems, and SSP is therefore an occurring polymerization mechanism in HTP above T_p, which contributes to the amorphous fractions of our hydrothermally synthesized polyimides (Scheme 4B,C).

While the amorphous fraction from polymerization during heating cannot be avoided, it should be possible to avoid the SSP pathway. Two approaches are thinkable. The first and more obvious approach is to perform HTP at $T_R < T_P$. We performed HTP at T_R = 140 °C for *p*(PDA-BTA) ($T_p([H_2PDA^{2+}BTA^{2-}])$ = 149 °C), and 160 °C for *p*(Bz-BTA) ($T_p([H_2Bz^{2+}BTA^{2-}])$ = 172 °C). The resulting diffractogams of both systems, superposed with the diffractograms of polyimides obtained at 200 °C, are depicted in Fig. 3. We note

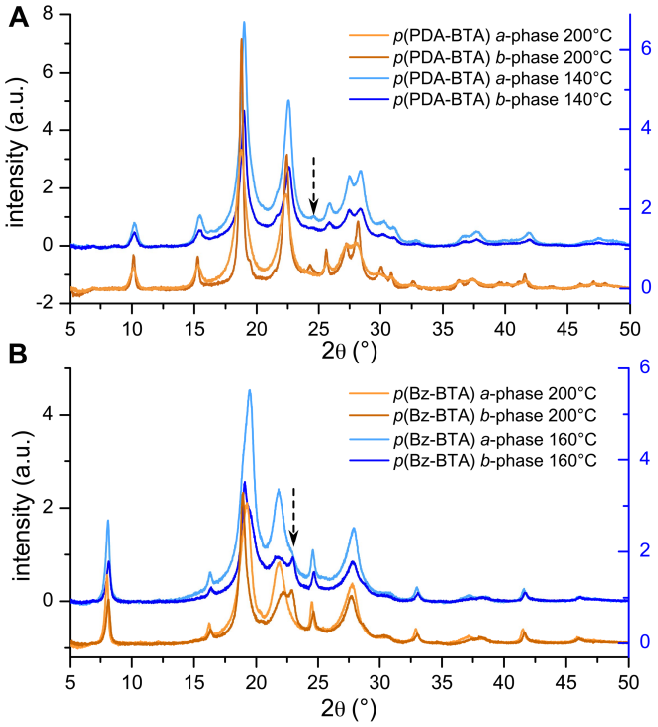

Fig. 3 this figure caption has been changed Powder-diffractograms of the dried *a*- and *b*-phases after HTP at T_R below T_p (t_R = 12 h); **A:** *p*(PDA-BTA); **B:** *p*(Bz-BTA).

that (*i*) the crystallinity of the *a*-phases synthesized at $T_R < T_p$ has increased (Fig. 3, light blue curves). For *p*(PDA-BTA), *a*- and *b*-phase show the same reflexes and relative intensities. Most strikingly, the additional reflex that we only found in the *b*-phases at all t_R synthesized at 200 °C (24° (2θ)), indicated by an arrow in Fig. 3A) is now also present in the *a*-phase. For *p*(Bz-BTA), this effect is less pronounced. The additional reflex (23.5° (2θ)) that was only observed in the *b*-phases for T_R = 200 °C now starts to appear as a shoulder in the *a*-phase (indicated by an arrow in Fig. 3B). (*ii*) The amorphous backgrounds are slightly higher, compared to the PIs synthesized at T_R = 200 °C. A crystalline and an amorphous PI can be considered as the thermodynamic and the kinetic product, respectively. For formation of the crystalline product, a relatively high energetic barrier has to be overcome (section **2.1**, Scheme 3). As the reaction system can more readily supply this activation energy at higher than at lower temperatures and pressures, the time required to obtain the crystalline product is lower for higher than for lower T in the HT regime. Consequently, the crystallinity obtained in HTP for a given reaction time scales with the reaction temperature. We thus believe that the increase of the amorphous fraction is related to the important temperature difference (140 and 160 *vs.* 200 °C). Taking this temperature difference into account, it is even more

impressive that the difference in diffractograms of the *a*- and *b*-phases is much less pronounced for $T_R < T_p$. Even more striking is the effect of SSP suppression on the morphology of the obtained PIs (section **2.3**).

2.3 Morphology in HTP – Effect of sHT and SSP pathways

SEM analysis of PIs synthesized at $T_R < T_p$ reveals that lowering the reaction temperature generates impressive morphological homogeneity (Fig. 4). *p*(PDA-BTA) still shows cauliflower-like morphologies in the *a*-phase (Fig. 4A), but the particle size distribution is much narrower when synthesized at $T_R < T_p$ than at $T_R > T_p$ (see ESI† for overview images). The *p*(PDA-BTA) *b*-phase is now exclusively composed of micro flowers, again all in a quite narrow size range (Fig. 4B and ESI†). *p*(Bz-BTA) is composed of flat microflowers with rounded platelets, which are decorated with smaller platy crystallites at their rims (Fig. 4C), as observed for $T_R = 200$ °C and the *b*-phase is exclusively composed of very homogeneous microflowers (Fig. 4D) of *ca.* 2 μm in diameter that aggregate to bigger particles (ESI†).

Clearly, avoiding SSP has a strong impact on the morphological homogeneity: both size and shape distribution are much narrower compared to HTP carried out at 200 °C. The strong effect on the PI products' morphological homogeneity can be fully explained by suppression of the SSP pathway. PIs formed *via* HTP are – as any crystallizing species – prone to crystallize on an external nucleus. We have previously shown that the SSP of monomer salt crystallites leads to precise copies of the monomer salt crystallites' form.[12] Given the inhomogeneous size and shape of both monomer salts (*cf.* Fig. 1), copying of these particles *via* SSP leads to a broad size and shape distribution of PI particles, on which hydrothermally formed PIs then crystallize (Scheme 5). By suppressing SSP, the only PI nuclei already present are the spherical PI particles obtained *via* sHTP. As sHTP takes place in a rather narrow time window (t_h is estimated to be 30 - 40 min), the amorphous PI particles resulting from sHTP have themselves a narrow size distribution. Consequently, the growth of PIs formed *via* HTP on these spherical PI particles from sHTP leads to spherical objects decorated with platelet-shaped PI crystallites of narrow size distribution (Scheme 5).

Finally, we performed a last set of experiments to avoid SSP. In this approach we changed the monomer salt concentration, *i.e.* we performed additional experiments with lower (0.015 $^{mol}/_{L}$) and higher (0.05 $^{mol}/_{L}$) concentration than our typical concentration of 0.03 $^{mol}/_{L}$, but worked again at $T_R > T_p$. The reasoning behind this approach is that SSP can only occur, if solid, non-dissolved monomer salt crystallites are present. Thus, if one uses a concentration so small that the entire monomer salt dissolves rapidly, there are no monomer salt

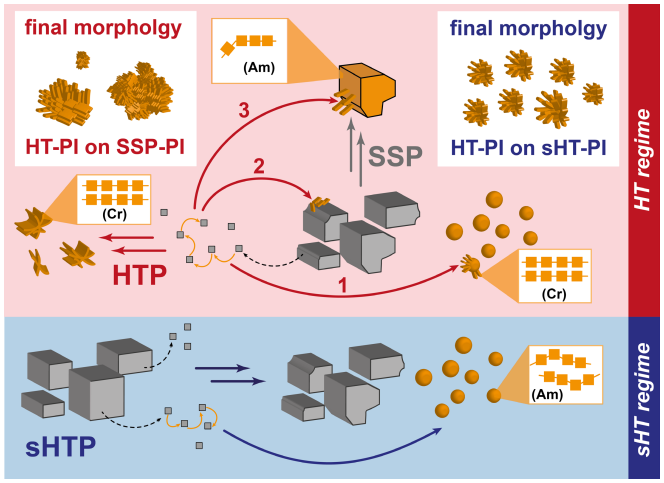

Scheme 5 Morphological implications of coexistence of sHTP, HTP and SSP. **bottom:** During heating (in the sHT regime, blue box), a part of the monomer salt dissolves and polymerizes in solution. The PI particles formed *via* sHTP are spherical, of narrow size distribution and amorphous (Am). **top:** In the HT regime, PI forms by HTP. The resulting PI particles are crystalline (Cr) and depict flower-shaped morphologies. PIs formed *via* HTP will use preexisting spherical particles (from sHTP) as nuclei and crystallize on them (pathway **1**). The final morphology of HT-PI on sHT-PI are spherical particles decorated with platy crystals of narrow size distribution. If $T_R > T_p$, SSP takes place in parallel. PI particles from SSP are obtained as copies of the remaining monomer salt particles, and are amorphous (Am). PIs formed *via* HTP will also use PI particles from SSP as nucleation seeds (pathway **3**), which generates shape-inhomogeneous particles decorated with platy crystals of a rather broad size distribution.

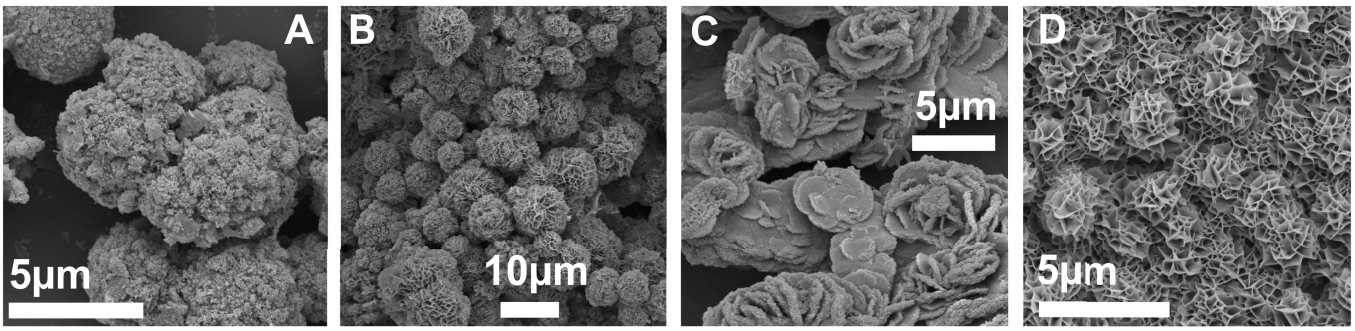

Fig. 4 SEM images of the dried *a*- and *b*-phases after HTP at T_R below T_p (t_R = 12 h); **A:** *p*(PDA-BTA), *a*-phase; **B:** *p*(PDA-BTA), *b*-phase; **C:** *p*(Bz-BTA), *a*-phase; **D:** *p*(Bz-BTA), *b*-phase.

crystallites left to undergo SSP. Note that a small concentration should lead to the complete dissolution of the respective monomer salt, but not to its complete polymerization in the sHT regime: the extent of sHTP is – as any reaction – limited by the reaction rate. Thus, if all monomer salt dissolves in the sHT regime, it will only polymerize to some extent *via* sHTP. Moreover, this set of experiments should clarify if indeed suppression of SSP at $T_R < T_p$, and increasing crystallinity *via* HTP with increasing T_R are counteracting events. Using lower concentrations but the relatively high T_R of 200 °C should achieve morphological homogeneity (by suppression of SSP and avoiding amorphous PI nuclei of broad size and shape distribution), and increase crystallinity (as carried out at the relatively high T_R = 200 °C). Indeed, by lowering the concentration, we achieve impressive morphological homogeneity, as we obtained by lowering the reaction temperature (for SEM images, see ESI†). The diffractograms obtained *via* XRD for different concentrations of the two systems are plotted in Fig. 5. As the *b*-phases are little affected by t_R and T_R (ESI†) we discuss only the effect on the *a*-phases.

The amorphous fractions for $c = 0.05\ ^{mol}/_{L}$ (yellow areas) are bigger than for $c = 0.03\ ^{mol}/_{L}$ (orange areas), which are bigger than for $c = 0.015\ ^{mol}/_{L}$ (red areas), for both PIs. It becomes clear, that the qualitative amount of amorphous fraction does indeed increase with increasing concentration. The extent of amorphous fraction decreases most between $c = 0.05\ ^{mol}/_{L}$ and $c = 0.03\ ^{mol}/_{L}$, in both cases, and only little between $c = 0.03\ ^{mol}/_{L}$ and $c = 0.015\ ^{mol}/_{L}$.

In combination with HTP carried out below T_p of each system, these experiments strongly support the hypotheses of: (*i*) SSP occurring at $T_R > T_p$, (*ii*) SSP accounting in part for the amorphous product components, (*iii*) morphological homogeneity by avoiding SSP, and (*iv*) higher crystallinity of the final polyimides with increasing temperature in the hydrothermal regime.

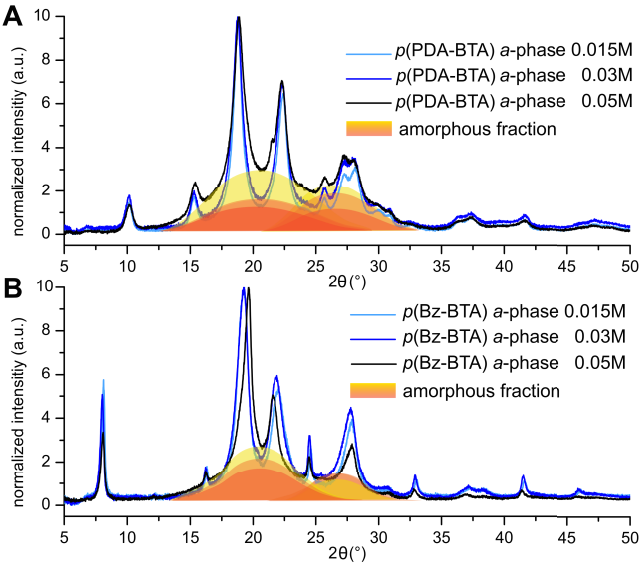

Fig. 5 This figure has been changed Powder-diffractograms of the dried *a*- and *b*-phases after HTP at T_R below T_p (t_R = 12 h) and at different concentrations; **A:** *p*(BTA-PDA); **B:** *p*(BTA-Bz).

3 Conclusions

In this contribution we developed a global picture of hydrothermal polymerization of polyimides. Our model considers different polymerization mechanisms that all take place during the HTP experiment (namely sub-hydrothermal polymerization, sHTP, hydrothermal polymerization, HTP, and solid-state polycondensation, SSP). The model further includes the reaction parameters that determine if and to what extent the different polymerization pathways take place, and relates the reaction parameters to physicochemical properties of the precursors, *i.e.* the corresponding monomer salts. Thereby, we can relate the extent of sHTP to the solubility of the monomer salt in the sHT regime, and the extent of SSP to the reaction temperature with respect to T_p of the corresponding monomer salt. Due to our experimental set-up sHTP cannot be avoided, as the autoclave inevitable passes the sHT regime during heating. However, we designed two sets of experiments to avoid SSP. These experiments show, that the suppression of SSP creates impressive morphological homogeneity, and decreases the amorphous PI fraction. We believe that this contribution presents a big step towards a global understanding of hydrothermal polymerization of polyimides. The precise knowledge of all parameters discussed herein, should allow for the design of HTP experiments that enable to crystallize any polyimide.

Acknowledgements

The authors acknowledge TU Vienna for funding this project. Powder X-ray diffraction measurements were carried out at the X-Ray Center of TU Vienna, and SEM was carried out at the inter-faculty electron microscopy facility of TU Vienna (USTEM). B.B. is holder of an excellence fellowship of TU Vienna. The authors would like to thank Catarina I. O. Martins, Sebastian España-Orozco and Philipp Hans for assistance with XRD measurements, and are indebted to Jörg Menche and Jakob Hayden for many fruitful discussions.

References

1 W. Volksen, R. D. Miller and G. Dubois, *Chemical reviews*, 2009, **110**, 56–110.
2 S. Shian and K. H. Sandhage, *Review of Scientific Instruments*, 2009, **80**, 7.
3 T. Hirai, M. J. Cole, M. Fujii, S. Hasegawa, T. Iwai, M. Kobayashi, R. Srama and H. Yano, *Planetary and Space Science*, 2014, **100**, 87–97.
4 P. M. Hergenrother, *High Performance Polymers*, 2003, **15**, 3–45.
5 M. E. Rogers and T. E. Long, *Synthetic methods in step-growth polymers*, Wiley Online Library, 2003.
6 M. Ree, S. Swanson and W. Volksen, *Polymer*, 1993, **34**, 1423–1430.
7 K. Kimura, K. Wakabayashi, S. Kohama and S. Yamazaki, *Polymer*, 2007, **48**, 458–466.
8 D.-J. Liaw, K.-L. Wang, Y.-C. Huang, K.-R. Lee, J.-Y. Lai and C.-S. Ha, *Progress in Polymer Science*, 2012, **37**, 907–974.
9 H. Frank, U. Ziener and K. Landfester, *Macromolecules*, 2009, **42**, 7846–7853.
10 K. Kurita, Y. Suzuki, T. Enari, S. Ishii and S.-I. Nishimura, *Macromolecules*, 1995, **28**, 1801–1806.
11 B. Baumgartner, M. J. Bojdys and M. M. Unterlass, *Polymer Chemistry*, 2014, **5**, 3771–3776.
12 M. M. Unterlass, F. Emmerling, M. Antonietti and J. Weber, *Chemical Communications*, 2014, **50**, 430–432.
13 M. M. Unterlass, D. Kopetzki, M. Antonietti and J. Weber, *Polymer Chemistry*, 2011, **2**, 1744–1753.
14 M. M. Unterlass, *Materials Today*, 2015, in press, DOI: 10.1016/j.mattod.2015.02.013.
15 P. J. Flory, *Principles of polymer chemistry*, Cornell University Press, 1953.
16 G. F. Sykes and A. K. St Clair, *Journal of applied polymer science*, 1986, **32**, 3725–3735.
17 H. Kita, T. Inada, K. Tanaka and K.-i. Okamoto, *Journal of membrane science*, 1994, **87**, 139–147.
18 T.-K. Ahn, M. Kim and S. Choe, *Macromolecules*, 1997, **30**, 3369–3374.
19 J. Seo and H. Han, *Polymer degradation and stability*, 2002, **77**, 477–482.
20 Y. Xu, C. Chen, P. Zhang, B. Sun and J. Li, *Journal of applied polymer science*, 2007, **103**, 998–1003.
21 O. M. Yaghi, M. O'Keeffe, N. W. Ockwig, H. K. Chae, M. Eddaoudi and J. Kim, *Nature*, 2003, **423**, 705–714.
22 A. P. Cote, A. I. Benin, N. W. Ockwig, M. O'Keeffe, A. J. Matzger and O. M. Yaghi, *science*, 2005, **310**, 1166–1170.
23 H. M. El-Kaderi, J. R. Hunt, J. L. Mendoza-Cortés, A. P. Côté, R. E. Taylor, M. O'Keeffe and O. M. Yaghi, *Science*, 2007, **316**, 268–272.
24 H.-K. Lyeo and D. G. Cahill, *Physical Review B*, 2006, **73**, 144301.